Zr metal preparation method using ZrCl as medium via chloride-based electrorefining and thermal decomposition reaction

Jungho Hur [a], Hyeongjin Byeon [b], Kiwon Kang [a], Eunyeong Choi [a], Jaeyeong Park [a*]
[a]*Department of Nuclear Engineering, Ulsan National Institute of Science and Technology, 50 UNIST-gil, Ulju-gun, Ulsan 44919, Republic of Korea*
[*]*Corresponding author: jypark@unist.ac.kr*

1. Introduction

Zirconium metal recovery technology from Zr-based alloy (e.g., cladding, pressure tube etc.) has been studied by using chloride-based electrorefining [1]. Electrochemical behavior of Zr is basically complicated in chloride-based salt with two soluble states of Zr^{4+}/Zr^{2+} and insoluble states of Zr0/ZrCl. Furthermore, there were limitations previous method of direct Zr metal recovery in molten salts. Disproportionate reaction ($Zr+Zr^{4+}\leftrightarrow Zr^{2+}$), low concentration of $ZrCl_4$ (1 wt.%) in electrolytes and powdery Zr deposits restrain the throughput of process. The purity of Zr deposit is also influenced by ZrCl co-deposition. To overcome the disadvantages of direct Zr metal recovery method, two step Zr metal recovery process using ZrCl as medium is designed and experimentally investigated in this study.

2. Experimental

All experiments of electrolysis and thermal decomposition were performed in the Ar-atmosphere glovebox (Korea Kiyon, KK-021AS) with concentration of O_2 and H_2O < 0.1 ppm.

2.1 Electrolysis

Anhydrous LiCl-KCl eutectic salt and $ZrCl_4$ (Sigma-Aldrich, 99.99%) were melted and prepared as 10 wt% of $ZrCl_4$. The electrolytes were diluted to 2 wt% of $ZrCl_4$ for preventing loss of $ZrCl_4$ by sublimation. Electrodes with different diameter were inserted in the cell to ensure that the surface of counter electrodes is larger than working electrode. One tungsten rod (Alpha Aesar, 99.99%) with a diameter of 3.175 mm was used as working electrode and two tungsten rods (Alpha Aesar, 99.99%) were selected as counter electrode. Operation temperature was set as 450 ℃ and applied potential on working electrode was -1.1 V (vs. 1 wt% Ag/AgCl). The real-time monitoring and controlling of electrochemical cell were conducted by AMETEK Solartron 1287A with CorrWare software. The experiments were repeatedly performed to

2.2 Pyridine washing

ZrCl deposits were rinsed with anhydrous pyridine (Sigma-Aldrich, 99.8%) to remove adhered electrolytes for observation of clear change between ZrCl and Zr metal. Rinsed ZrCl were put into a vacuum atmosphere mini chamber of glove box to removing residual pyridine.

2.3 Thermal decomposition

A vacuum distillation furnace was built in a same glove box operating electrolysis. The furnace was composed of two sections, a reactor and retrieval section. Tantalum crucible with a diameter of 30 mm and a height of 40 mm containing ZrCl sample were introduced in a reactor section surrounded by heating furnace. The temperature was controlled by a proportional-integral-derivative (PID) system in the furnace. The speed of temperature increase was 200 K/h for all experiments and the rate of decrease was in the range from 0.04-0.06 K/s. The pressure was controlled in two conditions, atmospheric pressure and 1.7-1.8 torr.

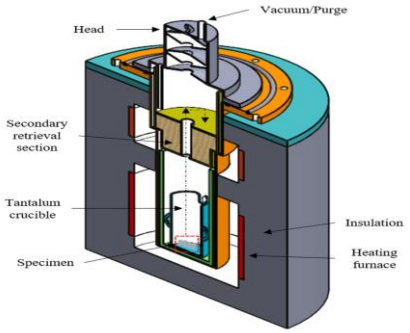

Fig. 1. Schematic diagram of vacuum distillation furnace

A test matrix of thermal decomposition for investigating of thermal decomposition mechanism and optimized condition is shown in table 1.

Table 1: Thermal decomposition test matrix

Test ID	Temp. (℃)	Pressure (torr)	Reaction time (h)
TD-1	600	Atmospheric pressure	12
TD-2		1.7-1.8	12
TD-3			24
TD-4	800	Atmospheric pressure	12
TD-5		1.7-1.8	12
TD-6			24
TD-7	1100	Atmospheric pressure	12
TD-8		1.7-1.8	12
TD-9			24

3. Results

3.1 Electrolysis

As mentioned above, the electrodeposition of ZrCl for enough amount were repeated in identical experimental setup. The averaged current response and charge transfer for electrolysis of 100000 s (27.8 h) were measured. The current of all experiments was in the range of ~40–60 mA. Charges of ~4500–6000 C, equivalent to ~1.97–2.63 g of ZrCl, were passed in each experiment.

ZrCl was collected without any dendritic morphology and detached particles at the bottom of electrochemical cell. The crystallographic and microstructural characteristics of the electrodeposited ZrCl were analyzed by XRD, SEM and FIB. Fig. 2 shows the optical image of ZrCl deposited on the tungsten cathode, SEM image of ZrCl powder, and FIB cut cross sectional image. A flat-layered morphology of ZrCl was confirmed by FIB cut cross-sectional SEM/EDS analysis of ZrCl. Electrolytes were trapped between stacked ZrCl layers, also covering ZrCl deposits. The atomic ratio between Zr, Cl, and K was revealed by EDS point analysis as shown in Table 2.

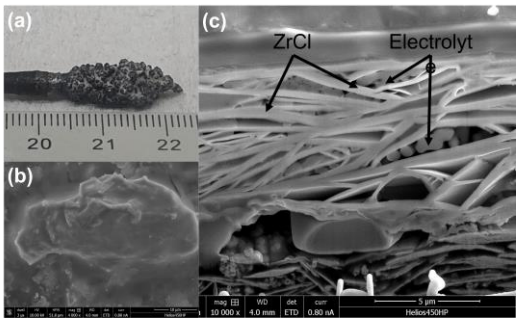

Fig. 2. Optical image of electrodeposited ZrCl, (b) ZrCl powder, and (c) FIB cross-sectional image of ZrCl.

Table 2. FIB cut cross-sectional EDS analysis of ZrCl

Atomic ratio (%)	Zr	Cl	K
ZrCl section	48.21	48.46	3.33
Electrolyte section	9.92	44.76	45.32

We analyzed that only ZrCl was recovered in a given electrochemical system as shown in Fig. 3. Also, LiCl which is soluble to pyridine were well removed by rinsing. However, KCl remained adhered to the depositions due to low solubility.

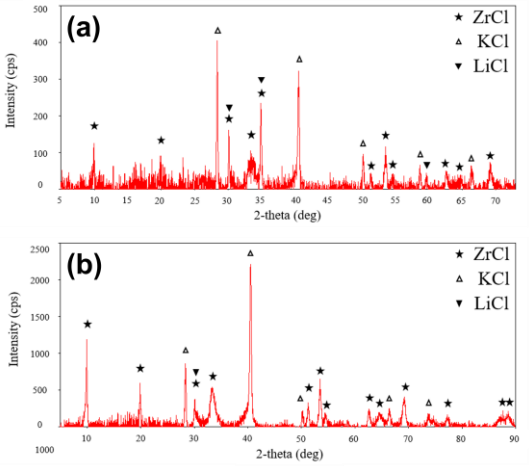

Fig. 3. XRD pattern of electrodeposited ZrCl (a) before and (b) after pyridine rinsing.

3.2 Thermal decomposition

At a temperature of 600 ℃, as shown in Fig. 4, no ZrCl peak was found in the XRD pattern of the Zr product after thermal decomposition of ZrCl. The lower the reaction pressure and the longer the reaction time, the more distinguishable the Zr metal peaks. Therefore, it can be assumed that thermal decomposition occurred, but the crystallization of the Zr metal was not sufficient. HCP-Zr metal peaks were identified in TD-1 and TD-2. However, the FCC-Zr metal peak was visible in TD-3. In addition, in TD-1 to TD-3, KCl remained after the thermal decomposition reaction. When the temperature was raised to 800 ℃, the peak of Zr metal appeared more clearly at 600 ℃, which is shown in Fig. 5, it means that the crystallization process of Zr metal is better developed. KCl peak. Even in TD-6, the KCl peak completely disappeared. For TD-4 and TD-5, HCP-Zr and FCC-Zr metal peaks were identified together. However, in TD-6, only FCC-Zr metal peaks were identified with increasing mean height. In all cases where the temperature was 1100 ℃, the FCC-Zr metal peak appeared without the KCl peak as shown in Fig. 6.

Particles evolved from TD-1 and TD-2 in Fig. 4 have rectangular and circular shapes, respectively, in a layered structure such as a basement. The particle size was about 0.5 μm in TD-1 and less than 0.1 μm in TD-2. The lower pressure conditions appear to have created more nucleation points allowing for finer particle evolution. The particles became larger due to improved growth and merging with each other.

The layer structure observed at 800 ℃ to 600 ℃ was completely broken as shown in Fig. 5. Almost all of the particles were very fine, some reached a size of 2-4 μm. In general, particles are well developed and are connected to neighboring particles. In TD-6, the specificity and independence of the particles stood out.

At 1100 ℃ in Fig. 6, round-shaped crystals with clean surfaces were observed under all conditions, especially under low pressure conditions. The crystallinity of the particles was good, and the degree of agglomeration was relatively low compared to other cases.

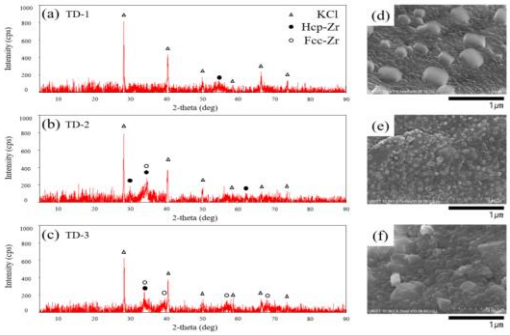

Fig. 4. XRD pattern of (a) TD-1, (b) TD-2, (c) TD-3, and SEM image of (d) TD-1, (e) TD-2, (f) TD-3.

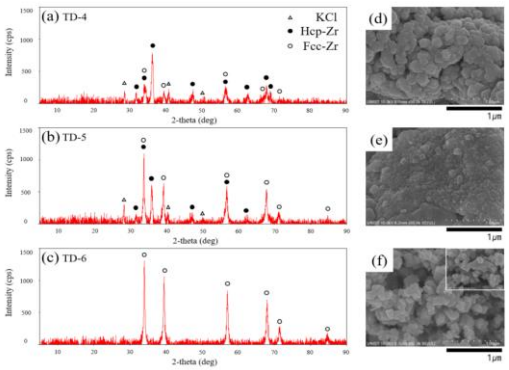

Fig. 5. XRD pattern of (a) TD-4, (b) TD-5, (c) TD-6, and SEM image of (d) TD-4, (e) TD-5, (f) TD-6.

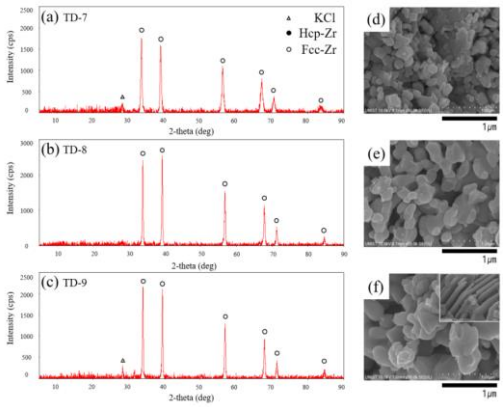

Fig. 6. XRD pattern of (a) TD-7, (b) TD-8, (c) TD-9, and SEM image of (d) TD-7, (e) TD-8, (f) TD-9.

After washing with pyridine, KCl was the only remaining electrolyte. In all cases, the concentration of K representative of the residual electrolyte after the electrolysis was determined by ICP-OES, and the results are shown in Fig. 8. As the process increases and the pressure decreases, the amount of distilled K increases. Distillation of the electrolyte is effective enough to improve the purity of Zr metal to high levels at 800 ℃, 1.7-1.8 torr and 24 hours and 1100 ℃, 1.7-1.8 torr and over 12 hours

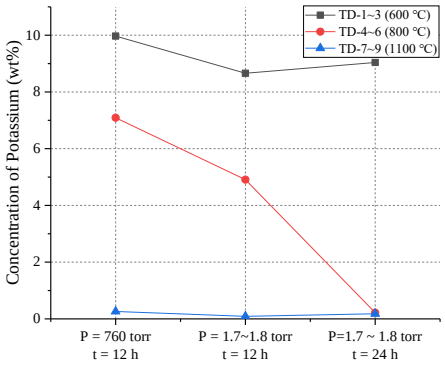

Fig. 7. Concentration profile of potassium in samples after thermal decomposition.

4. Discussion

4.1 Zr metal verification

The crystalline phase of the Zr metal sample was identified by XRD pattern. However, FCC-Zr did not appear in the temperature-pressure equilibrium diagram of Zr, whereas HCP and BCC steps have a high probability under the conditions used in this study. In addition, the XRD library data of FCC-Zr was similar to zirconium oxide, leading to uncertainty in the identification of zirconium metal. To confirm this, the spectrum of the sample was obtained by applying Raman spectroscopy and then compared with the published ZrO_2 spectrum and that of a commercially available ZrO_2 powder (Sigma-Aldrich, 99%). Four samples (TD-4,6,7,9) representative of the Zr metal produced in this study and one Zr sample heat treated at 1100 ℃, 1.7-1.8 torr and over 12 hours were selected for analysis. The Raman spectrum obtained from ZrO_2 showed many peaks similar to those of previous studies as shown in Fig. 10, but there was no peak in the pyrolyzed Zr spectrum [2]. Furthermore, the results for the prepared Zr metal are consistent with previous studies that reported spectra of pure Zr [3].

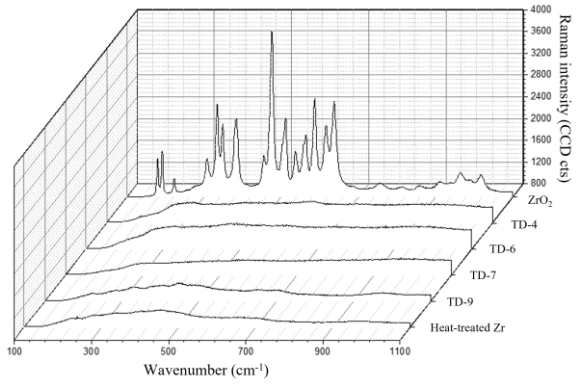

Fig. 8. Raman spectrum comparison between thermal decomposition samples and ZrO_2.

4.2 Thermal decomposition mechanism of ZrCl

When the reaction took place, the Zr metal structure began to evolve on the surface of the ZrCl deposited structure. The reaction rate was affected by temperature and atmospheric pressure. The lower the pressure and the higher the temperature, the faster the reaction rate. It was also assumed that the crystalline phase of Zr metal was stabilized as FCC-Zr. FCC-Zr is in a metastable state between HCP and BCC as determined not only from the cold rolling effect but also from as-cast zircaloy-4. Similar to other pure metals such as Hf, Co, Ti, and Ag, the metastable phase of FCC-Zr is likely to be formed by distortion of the lattice due to the high strain of the crystal structure reported through experiments. During the heating process, a maximum of 1,373K HCP-Zr is transformed into BCC-Zr, and defects such as dislocations and grain boundaries due to Zr anisotropy are accumulated. To accommodate these defects within the crystal structure, BCC-Zr has the potential to be converted to FCC-Zr, which is more favorable for defects to migrate because of lower stacking defect energy and more free dislocation slip and glide. The operating pressure also appears to affect the crystal structure of the recovered metal Zr. As the mixture of LiCl-KCl evaporates more, HCP or BCC becomes thermodynamically unstable due to the higher stacking fault energy compared to FCC-Zr. A mixture of LiCl-KCl can be present in the grain boundary region of the ZrCl precipitate to form metallic Zr, thus forming FCC-Zr to form ZrCl, LiCl, and KCl.

For comparison with the results obtained in this study, the same experiment was performed using a commercial Zr powder (Sigma-Aldrich, 100-mesh). The above phenomenon was also observed. As shown in Figure 9, only HCP-Zr was found in the samples. However, the peak height of HCP-Zr decreased sharply under low pressure and high temperature conditions. FCC-Zr was confirmed after heat treatment under the same conditions. The height of the HCP-Zr peak decreased with increasing heat treatment time. In the SEM image, the twin structure and porous morphology of Zr metal powder were observed after heat treatment.

A similar structure can also be seen in Figs. 5f and 6f. The porous morphology was likely induced by $ZrCl_4$ gas evolution during the decomposition of ZrCl to Zr metal. The reaction between ZrCl, $ZrCl_4$ and Zr metal has been reported in the literature on ZrCl synthesis. A similar form was also found in the synthesis process of nano porous transition metals from the thermal decomposition reaction using dichalcogenide.

These results imply that thermal decomposition from ZrCl to Zr metal can be summarized as follows:

$$4ZrCl(s) \rightarrow ZrCl4(g)\uparrow + 3HCP{-}Zr(s) \rightarrow 3FCC{-}Zr(s) \quad (1)$$

When ZrCl is thermally decomposed above the activation temperature, the formation of HCP-Zr begins. The amount of Zr formed during the reaction increased. A twin structure formed between Zr metal crystals. Finally, twins were dominant in the metal powder and stabilized.

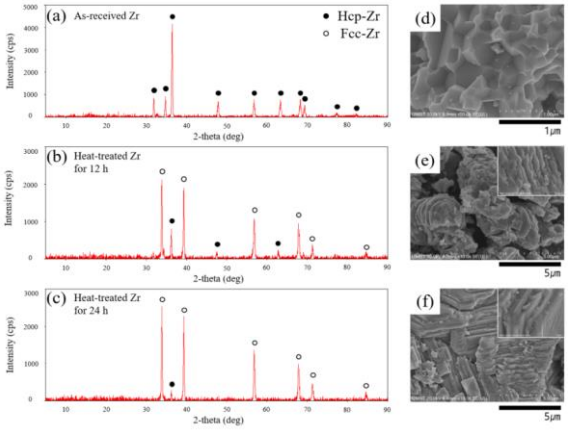

Fig. 9. XRD pattern of (a) as received Zr, (b) Heat-treated Zr for 12h, (c) Heat-treated Zr for 24h, and SEM image of (d) as received Zr, (e) Heat-treated Zr for 12h, (f) Heat-treated Zr for 24h.

5. Conclusions

Two step Zr recovery process using ZrCl as medium through electrodeposition in molten salt and thermal decomposition reaction was proposed and experimentally investigated. A microstructural and crystallographic analysis of electrodeposited ZrCl and thermally decomposed Zr metal from ZrCl were performed. The mechanism of thermal decomposition from ZrCl to Zr was also confirmed. The optimized condition of process was experimentally selected.

REFERENCES

[1] Sohn S, Park J, Hwang IS, Electrolytic recovery of high purity Zr from radioactively contaminated Zr alloys in

chloride salts. Int. J. Electrochem. Sci. 13(4) (2018) 3897–3909
[2] Cheema TA, Garnweitner G, Phase-controlled synthesis of ZrO2 nanoparticles for highly transparent dielectric thin films. CrystEngComm 16(16) (2014) 3366–3375
[3] Farina SB, Sanchez AG, Ceré S, Effect of surface modification on the corrosion resistance of Zr-2.5Nb as material for permanent implants. Procedia Mater. Sci. 8 (2015) 1166–1173